ELSEVIER

PII: S0032-3861(97)00011-6

Polymer Vol. 38 No. 19, pp. 4915–4923, 1997

0032-3861/97/$17.00 + 0.00

Prediction and manipulation of the phase morphologies of multiphase polymer blends: II. Quaternary systems

H.-F. Guo, N. V. Gvozdic and D. J. Meier*
Michigan Molecular Institute, Midland, MI 48640, USA
(Received 19 July 1996; revised 6 December 1996)

We have applied our model concerning the phase structures of multiphase polymer blends to quaternary blends of polyethylene, polypropylene, polystyrene and poly(methyl methacrylate) of different overall compositions. Predictions of the phase morphologies of such multicomponent blends are based on minimization of the total interfacial free energy of the system. We compare predictions of the model with experimental observations, and show agreement in every case between the predicted and experimental morphologies. Furthermore, we show that the phase structure of a quaternary blend can be converted from one type of phase morphology to another, e.g. from an encapsulation type to the dispersion type, by using an interfacially active block copolymer. This shows the possibility of adjusting the phase morphologies of multicomponent systems as desired. © 1997 Elsevier Science Ltd.

(Keywords: multiphase polymer blends; morphology; phase structure)

INTRODUCTION

Recently, there has been considerable interest in multiphase polymer blends which contain more than one minor phase. This interest is partially motivated by the commercial quest for new materials[1,2] with improved properties, such as ternary blends of two polymers with an impact modifier[3–5], but also motivated by the potential opportunity to recycle multicomponent commingled waste plastics without extensive separation[6–10].

In multicomponent polymer blends, morphological concerns involve not only the dispersed phase sizes and the interfacial adhesion, but also the phase structure of the system. Studies have shown that the dispersed phases in ternary blends can form either an encapsulation-type phase structure or remain as separately dispersed phases in the matrix (separation-type phase structure)[1,2]. Predictions of which morphology will form can be made on the basis of which phase morphology has the lowest interfacial free energy[11]. Since the mechanical properties of a multiphase blend are influenced by the phase morphology[7], an understanding and control of the phase structures of multiphase blends is very important. In order to enable prediction and control of the phase structure, we have extended our model[11] for the phase structure of ternary polymer blends to those of quaternary systems.

In this paper, we discuss the extended model and show its application to predict the phase structures of various quaternary blends containing high-density polyethylene (HDPE), polypropylene (PP), polystyrene (PS) and poly(methyl methacrylate) (PMMA). The comparison between predictions and experimental observations will be discussed. The effect of using a poly(styrene-*b*-ethylene) (S–E) block copolymer to change the phase structure of a quaternary blend will also be discussed.

* To whom correspondence should be addressed

THEORETICAL BACKGROUND

The total Gibbs free energy of a multicomponent system is given by[11]

$$G = \sum_i n_i \mu_i + \sum_{i \neq j} A_i \gamma_{ij} \tag{1}$$

where G is the Gibbs free energy, n_i and μ_i are the number of moles and chemical potential, respectively, of component i, A_i is the interfacial area, and γ_{ij} the interfacial tension between the i and j components. Since the chemical potentials of a given system are independent of the phase morphology, the second term in equation (1), $\Sigma A_j \gamma_{ij}$, which represents the total interfacial free energy of the system, determines the system free energy and hence the equilibrium phase structure.

For a quaternary system with A as the matrix and B, C and D as minor phases, the number of possible interfaces m is six, using equation (2)[11], with the number of components N being 4,

$$m = \frac{N!}{2!(N-2)!} \tag{2}$$

However, from minimization of the interfacial free energy $\Sigma A_i \gamma_{ij}$, only three of the six possible interfaces can coexist in the system. Therefore, we can calculate from the following equation[11] that there are a total of 16 possible phase structures in a quaternary system of any

given composition:

$$q = N\left(\frac{m!}{(N-1)![m-(N-1)]!} - \frac{N[m-(N-1)]!}{(N-1)![m-2(N-1)]!}\right) \quad (3)$$

Since the equilibrium phase structure of the system will be the one which has the lowest interfacial free energy $\Sigma A_i\gamma_{ij}$, the prediction of the phase structure of a quaternary blend requires comparing the values of $\Sigma A_i\gamma_{ij}$ of the 16 possible phase structures.

Figure 1 shows four of 16 possible phase structures of a quaternary A/B/C/D blend when A is the matrix:

(1) B, C and D form separate phases (B + C + D);
(2) the D phase is encapsulated by the C phase while the B phase stays separate (B + C/D);
(3) the C and D phases disperse separately in the B phase (B/(C + D));
(4) the B phase encapsulates the C phase while the C phase encapsulates the D phase (B/C/D).

The total interfacial energy of each structure can be expressed as

$$\left(\sum A_i\gamma_{ij}\right)_{B+C+D} = A_B\gamma_{AB} + A_C\gamma_{AC} + A_D\gamma_{AD} \quad (4)$$

$$\left(\sum A_i\gamma_{ij}\right)_{B+C/D} = A_B\gamma_{AB} + A_C\gamma_{AC} + A_D\gamma_{CD} \quad (5)$$

$$\left(\sum A_i\gamma_{ij}\right)_{B/(C+D)} = A_B\gamma_{AB} + A_C\gamma_{BC} + A_D\gamma_{BD} \quad (6)$$

$$\left(\sum A_i\gamma_{ij}\right)_{B/C/D} = A_B\gamma_{AB} + A_C\gamma_{BC} + A_D\gamma_{CD} \quad (7)$$

$\Sigma A_i\gamma_{ij}$ values for the different phase structures can be calculated from values of interfacial tensions and dispersed phases sizes, using the following equations:

$$\left(\sum A_i\gamma_{ij}\right)_{B+C+D} = (36\pi V_B^2)^{1/3}\left[n_B^{1/3}\gamma_{AB} + n_C^{1/3}x^{2/3}\gamma_{AC} + n_D^{1/3}y^{2/3}\gamma_{AD}\right] \quad (8)$$

$$\left(\sum A_i\gamma_{ij}\right)_{B+C/D} = (36\pi V_B^2)^{1/3}\left[n_B^{1/3}\gamma_{AB} + n_C^{1/3}(x+y)^{2/3}\gamma_{AC} + n_D^{1/3}y^{2/3}\gamma_{CD}\right] \quad (9)$$

$$\left(\sum A_i\gamma_{ij}\right)_{B/(C+D)} = (36\pi V_B^2)^{1/3}\left[n_B^{1/3}(1+x+y)^{2/3}\gamma_{AB} + n_C^{1/3}x^{2/3}\gamma_{BC} + n_D^{1/3}y^{2/3}\gamma_{BD}\right] \quad (10)$$

$$\left(\sum A_i\gamma_{ij}\right)_{B/C/D} = (36\pi V_B^2)^{1/3}\left[n_B^{1/3}(1+x+y+y/x)^{2/3}\gamma_{AB} + n_C^{1/3}(x+y)^{2/3}\gamma_{BC} + n_D^{1/3}y^{2/3}\gamma_{CD}\right] \quad (11)$$

where V_B, V_C, V_D are volumes of the B, C and D phases, respectively, n_B, n_C and n_D are particle numbers, and $x = V_C/V_B$, $y = V_D/V_B$. As we discussed in a previous paper[11], in making predictions of the phase structures we assume that the number of particles of the three minor phases is the same ($n_B = n_C = n_D = n$). We recognize that this is a highly idealized case, while in reality particle numbers or sizes of each component are largely controlled by kinetic effects through the interaction between particle break-up and coalescence which usually result in different particle numbers. However, since the total surface area of a dispersed phase depends on only the cube root of the particle number, hence the order of the interfacial energies of different phase structures is not very sensitive to the particle numbers of the dispersed phases. As a result, the assumption of the same number of particles should not significantly affect our predictions. Our results will show that the phase structures predicted based on this assumption are in excellent agreement with our experimental results. With the assumption of the same particle numbers, equations (8)–(11) become

$$\left(\sum A_i\gamma_{ij}\right)_{B+C+D} = (36\pi V_B^2)^{1/3}n^{1/3}\left[\gamma_{AB} + x^{2/3}\gamma_{AC} + y^{2/3}\gamma_{AD}\right] \quad (12)$$

$$\left(\sum A_i\gamma_{ij}\right)_{B+C/D} = (36\pi V_B^2)^{1/3}n^{1/3}\left[\gamma_{AB} + (x+y)^{2/3}\gamma_{AC} + y^{2/3}\gamma_{CD}\right] \quad (13)$$

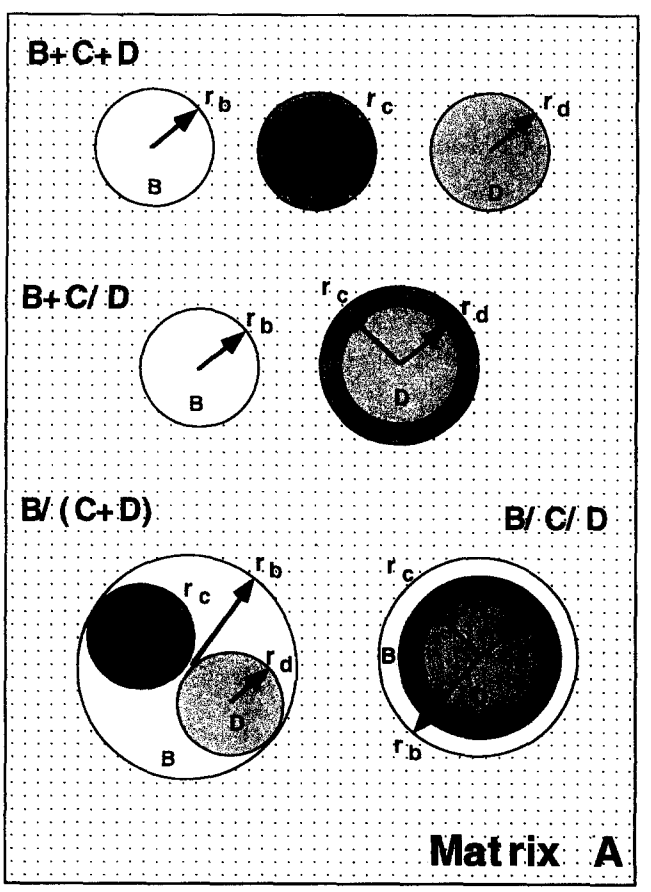

Figure 1 Schematic diagram showing 4 of 16 possible phase structures for a quaternary blend: (1) B, C and D phases remain separate (B + C + D); (2) the D phase is encapsulated by the C phase while the B phase stays separately (B + C/D); (3) the C and D phases disperse separately in the B phase (B/(C + D)); and (4) the B phase encapsulates the C phase while the C phase encapsulates the D phase (B/C/D)

Table 1 Interfacial tensions at 140°C (dyne cm^{-1})

PE/PS[a]	PE/PP[a]	PP/PS[a]	PE/PMMA[a]	PS/PMMA[a]	PP/PMMA[b]
5.9	1.1	5.1	9.7	1.6	8

[a] Measured values from Wu[12]
[b] Calculated values by using the harmonic-mean equation given by Wu[12]

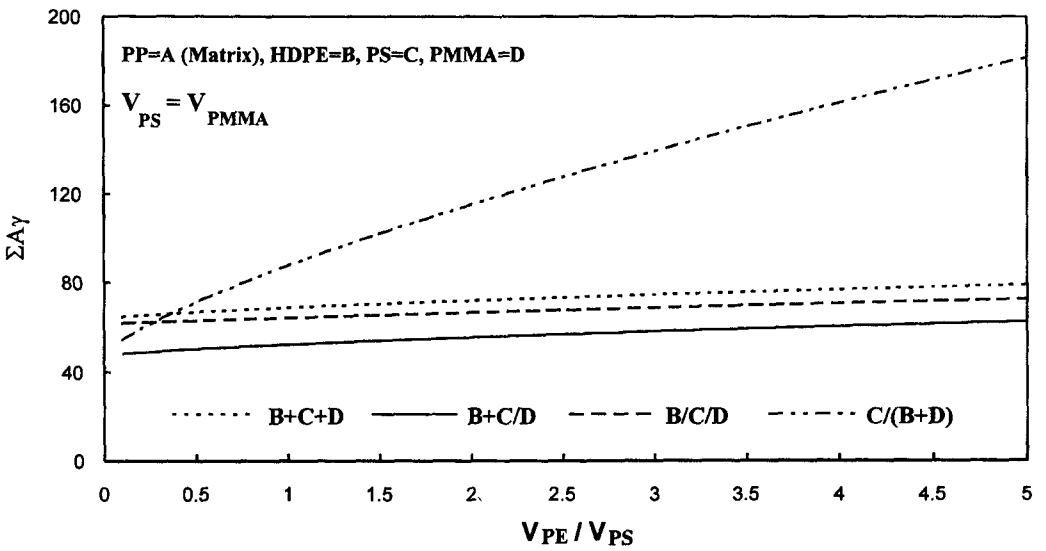

Figure 2 Interfacial energies ($\Sigma A_i\gamma_{ij}$) *versus* volume ratios of PE to PS (V_{PE}/V_{PS}) for quaternary blends of PP/HDPE/PS/PMMA where PP is the matrix component

$$\left(\sum A_i\gamma_{ij}\right)_{B/(C+D)} = (36\pi V_B^2)^{1/3} n^{1/3}\left[(1+x+y)^{2/3}\gamma_{AB} + x^{2/3}\gamma_{BC} + y^{2/3}\gamma_{BD}\right] \quad (14)$$

$$\left(\sum A_i\gamma_{ij}\right)_{B/C/D} = (36\pi V_B^2)^{1/3} n^{1/3}\left[(1+x+y+y/x)^{2/3}\gamma_{AB} + (x+y)^{2/3}\gamma_{BC} + y^{2/3}\gamma_{CD}\right] \quad (15)$$

Similar calculations can be carried out for the other analogous phase structures.

EXPERIMENTAL

The PS used in this study was Styron 666D from the Dow Chemical Company (M_W = 260 000 and M_n = 160 000). The HDPE was Tenite H6001-A from the Eastman Chemical Company with a melt index of 8.0. Isotactic PP was supplied by the Amoco Chemical Corporation (grade number 1046) with a melt index of 5.8. PMMA (M = 90 000) was obtained from Eastman Organic Chemicals, catalogue number 6036. S–E was synthesized in this laboratory by living sequential anionic polymerization[11]. It has a molecular weight of M_n = 73 000 and contains 50% PS.

All the blends were prepared by melt blending using a Haake Rheocord 90 torque rheometer with a 60 ml batch mixer equipped with a pair of roller blades. The mixer was preheated to the run temperature before the dry mixed blend components were added. All blending was at 200°C and 100 rpm for 10 minutes.

Figure 3 TEM micrograph of a PP/HDPE/PS/PMMA 60/20/10/10 blend (A = PP, B = HDPE, C = PS, D = PMMA)

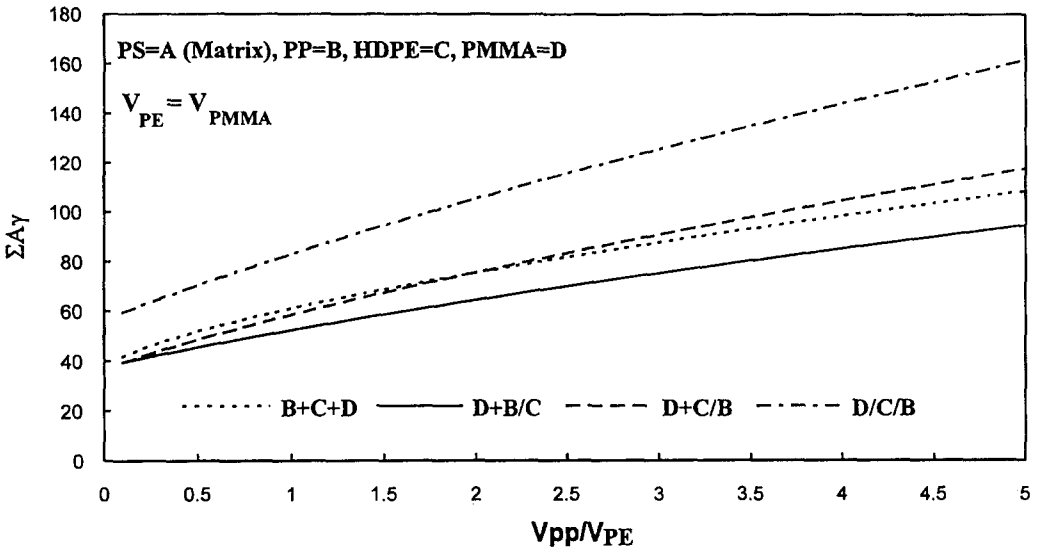

Figure 4 Interfacial energies ($\Sigma A_i \gamma_{ij}$) *versus* volume ratios of PP to PE (V_{PP}/V_{PE}) for quaternary blends of PS/PP/HDPE/PMMA where PS is the matrix component

Figure 5 (a) TEM micrographs of a PS/PP/HDPE/PMMA 60/20/10/10 blend; (b) SEM micrograph of the fracture surface of a PS/PP/HDPE/PMMA 60/20/10/10 blend. The fracture surface was etched with a methanol/water mixture (A = PS, B = PP, C = HDPE, D = PMMA)

After blending, the samples were quickly transferred to a Pasadena hydraulic press and compression moulded into sheets of 1.5 mm thickness. All moulding was carried out at 200°C and 300 psi for 5 min.

Figure 5 *(b)*

Scanning electron microscopy (SEM; model Amray 1820) and transmission electron microscopy (TEM; model Phillips EM301) were used to examine the morphologies of the blends. To prepare specimens for SEM, the compression-moulded sample sheets were fractured in liquid nitrogen, and the resulting fracture surfaces were then coated with gold and carbon. The fracture surfaces of some samples before being coated were etched with solvents to remove certain components to aid in identification. For TEM, ultrathin sections were cryomicrotomed from the compression-moulded sheets using an LKB 2088 microtome with a diamond knife. The sections were stained with ruthenium tetroxide (RuO_4) vapour for 30 min, which stained the PS phase but did not affect the PMMA phase. The PP and HDPE phases were partially stained by the RuO_4, but to different degrees.

RESULTS AND DISCUSSION

The interfacial tension data used in interfacial energy

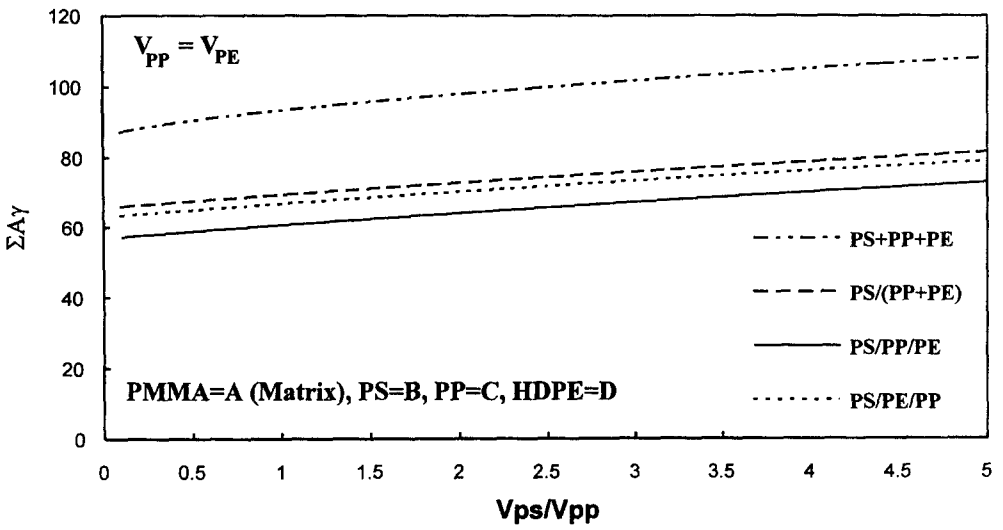

Figure 6 Interfacial energies ($\Sigma A_i\gamma_{ij}$) *versus* volume ratios of PS to PP (V_{PS}/V_{PP}) for quaternary blends of PMMA/PS/PP/HDPE where PMMA is the matrix component

Figure 7 (a) TEM micrograph of a PMMA/PS/PP/HDPE 60/20/10/10 blend; (b) SEM micrograph of the fracture surface of a PMMA/PS/PP/HDPE 60/20/10/10 blend. The fracture surface was etched with cyclohexane (A = PMMA, B = PS, C = PP, D = HDPE)

($\Sigma A_i\gamma_{ij}$) calculations are listed in *Table 1*. Most of them are from Wu's book[12]. Since no values of $\gamma_{PP/PMMA}$ were found, we calculated it by using the harmonic-mean equation[12]

$$\gamma_{12} = \gamma_1 + \gamma_2 - 4\left(\frac{\gamma_1^d\gamma_2^d}{\gamma_1^d + \gamma_2^d} + \frac{\gamma_1^p\gamma_2^p}{\gamma_1^p + \gamma_2^p}\right) \qquad (16)$$

Figure 7 *(b)*

where γ_{12} is the interfacial tension between 1 and 2, γ_1 and γ_2 are surface tensions, and γ^d and γ^p are non-polar and polar components of the surface tension, respectively. Values for γ, γ^d and γ^p are given by Wu[12].

Quaternary blends of PP, HDPE, PS and PMMA with PP as the matrix component were investigated. Values of $\Sigma A_i\gamma_{ij}$ were calculated for the 16 different phase structures and for various compositions, with some results shown in *Figure 2*. As mentioned above, equal particle numbers of the minor phases ($n_{PE} = n_{PS} = n_{PMMA}$) were used in these calculations. The phase structure (PE + PS/PMMA), where the PMMA phase is encapsulated by the PS phase and the PE particles are dispersed separately in the matrix, gives the lowest interfacial energy, and hence is predicted to be the preferred morphology. The TEM micrograph of *Figure 3* is for a PP/HDPE/PS/PMMA 60/20/10/10 blend, and shows that the morphology is exactly that predicted, i.e. all of the HDPE (B) particles (which have irregular shapes and spherulitic crystalline textures) are dispersed separately in the matrix, while all the PMMA (D) particles are encapsulated in the dispersed PS (C) phases. We realize that in *Figure 3* we have more PMMA particles than PS particles due to the complex kinetic

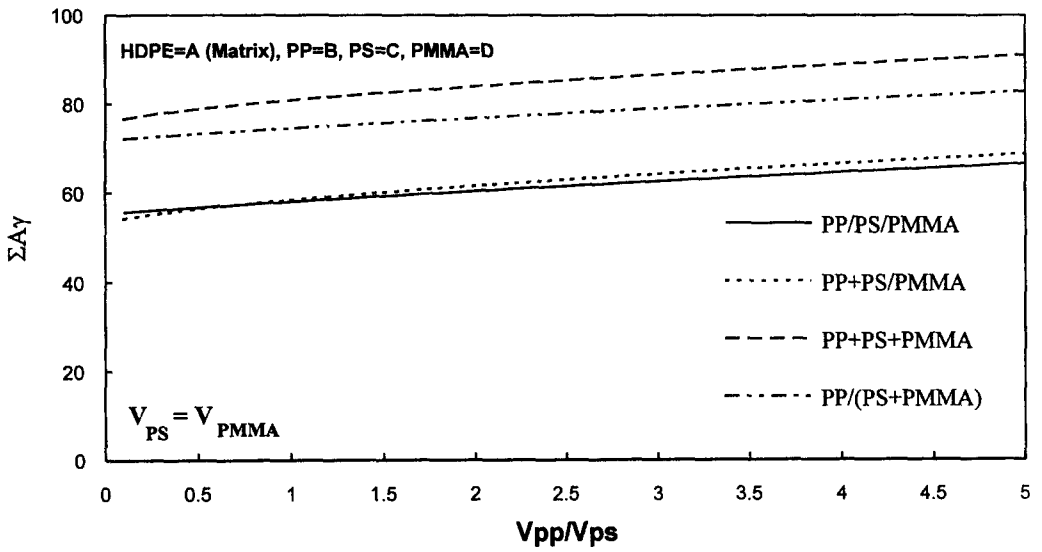

Figure 8 Interfacial energies ($\Sigma A_i\gamma_{ij}$) *versus* volume ratios of PP to PS (V_{PP}/V_{PS}) for quaternary blends of HDPE/PP/PS/PMMA where HDPE is the matrix component

effects, whereas in our calculations we have assumed the same particle numbers. Here the experimentally observed phase structure (which is always from non-equilibrium effects) agrees with the phase structure predicted from equilibrium considerations. This can be attributed to the dominating role played by interfacial tensions in determining the interfacial energy and the phase structure of the system. As a result, even during the blending process, which includes particle break-up and coalescence, the PMMA particles disperse in the PS phase rather than in the PP matrix because of the lower PMMA/PS interfacial tension ($\gamma_{PMMA/PS} = 1.6\,dyne\,cm^{-1}$ and $\gamma_{PMMA/PP} = 8\,dyne\,cm^{-1}$). On the other hand, the particle numbers which are determined by shear stresses, viscosities and interfacial tensions play only a minor role in influencing the energy level or the phase structure of the system, since the surface area of a dispersed phase depends on only the cube root of the particle number. The tendency for such a minimization is so strong that the phase structure having the lowest free energy level is formed even under the non-equilibrium mixing conditions[11]. This is true for all other results to be shown in the rest of this paper.

The calculated interfacial energies for some of these quaternary blends having PS as the matrix component are shown in *Figure 4*. These results predict that the phase structure of this system will be (PMMA+PP/HDPE), in which HDPE is encapsulated by PP and PMMA is separately dispersed in the matrix. *Figure 5a* shows that this prediction is completely confirmed by experiment. The figure shows a TEM micrograph of an ultrathin section of a PS/PP/HDPE/PMMA 60/20/10/10 blend. The small white or grey particles with diameters less than 1 μm in the matrix are PMMA particles (D). Also dispersed in the PS matrix are PP domains (B) with sizes varying from 1 μm to more than 10 μm. The HDPE particles (C), which have a spherulitic crystalline texture, are encapsulated by the PP phase. The white layers around the PP phases are not PMMA but holes generated by the microtome sectioning. Again, the morphology is a non-equilibrium one with many more PMMA particles than the others, but we still see an excellent agreement between experimental and predicted results as discussed above. The SEM micrograph of the fracture surface of this blend shown in *Figure 5b* leads to the same conclusions about the morphology. The fracture surface was etched with a methanol/water mixture to remove the PMMA, leaving many holes behind in the matrix. Encapsulation of HDPE (C) by PP (B) is also apparent in the micrograph.

Figure 6 shows some calculated interfacial free energy values $\Sigma A_i\gamma_{ij}$ for these quaternary blends having PMMA as the matrix component. The phase structure having the lowest total interfacial free energy is that of HDPE (D) encapsulated by PP (C) and PP encapsulated in turn by PS (B). Thus (PS/PP/HDPE) is the predicted phase structure. The phase morphology of a PMMA/PS/PP/HDPE 60/20/10/10 blend is shown in the TEM micrograph of *Figure 7a*. Dark layers of the PS phase (B) are found around the multiphase particles containing the PP (C) and HDPE (D) phases. The HDPE particles are at least partially encapsulated by the PP phase. The same phase structure is also observed in *Figure 7b*, which is an SEM micrograph of the fracture surface of the blend. Cyclohexane was used to etch the fracture surface to remove the PS. Gaps due to the removal of the PS shells between the PP (C) particles and the PMMA (A) matrix are seen, as marked by the arrow. The HDPE (D) phase is encapsulated by PP, as predicted.

Figure 8 shows predicted interfacial free energy values $\Sigma A_i\gamma_{ij}$ as a function of composition for the quaternary blends having HDPE as the matrix component. The results show that the predicted phase structure of the system will be influenced by the composition of the minor phases, in contrast to results for the other blend systems. When $V_{PP}/V_{PS} > 0.7$, the system prefers the phase structure (PP/PS/PMMA), whereas when $V_{PP}/V_{PS} < 0.7$ the system will prefer the phase structure (PP + PS/PMMA). *Figure 9a* shows the phase morphology of an HDPE/PS/PMMA 60/20/10/10 blend in which $V_{PP}/V_{PS} > 0.7$. It is clearly seen, as predicted, that all of the PMMA particles (D) are encapsulated by the PS (C), and that the PS phases are encapsulated by the PP phases (B). In contrast, *Figure 9b* shows the phase structure of an HDPE/PP/PS/PMMA 75/5/10/10 blend in which $V_{PP}/V_{PS} < 0.7$. As predicted, the structure is

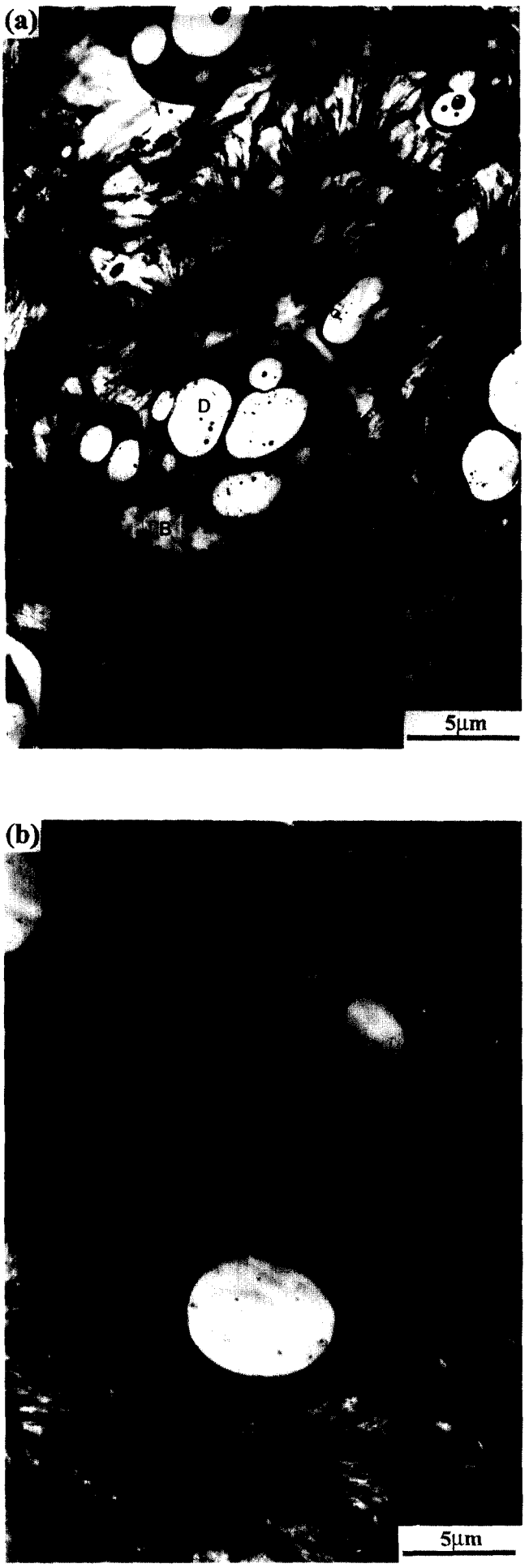

(PP + PS/PMMA), with PP no longer encapsulating the PS but forming a separate dispersed phase (albeit, partially residing at the PS interface). These results demonstrate that the phase morphology is affected by the composition of a blend, and hence morphologies cannot be predicted by consideration of interfacial tensions alone[2].

Figure 10 shows the interfacial free energy $\Sigma A_i\gamma_{ij}$ for a quaternary HDPE/PP/PS/PMMA 65/20/10/5 blend as a function of the interfacial tension $\gamma_{HDPE/PS}$ between PS and PE. When $\gamma_{PE/PS} > 5.7$ dyne cm^{-1}, the system will prefer a phase structure (PP/PS/PMMA), but when $\gamma_{PE/PS} < 5.7$ dyne cm^{-1}, the structure (PP + PS/PMMA) will be preferred. The data in *Table 1* show that $\gamma_{PE/PS}$ is 5.9 dyne cm^{-1}, thus predicting that the phase structure of this blend will be (PP/PS/PMMA). Since the value of $\gamma_{PE/PS}$ is only slightly above the predicted cross-over value of 5.7 dyne cm^{-1}, this suggests that this phase structure can be changed to (PP + PS/PMMA) by a modest decrease in $\gamma_{PE/PS}$. This can be done by adding an interfacially active block copolymer (S–E) to the system. *Figures 11* and *12* compare the phase structures without and with addition of the block copolymer. The phase morphology shown in *Figure 11* of the HDPE/PP/PS/PMMA 65/20/10/5 blend without the block copolymer is clearly one in which PMMA (D) is encapsulated by PS (C), and the PS encapsulated in turn by PP (B), as predicted. However, *Figure 12* shows the morphology of the same blend system to which 0.5% S–E block copolymer has been added. Now the PS (C) phase size has been reduced by the addition of the S–E, and most of the PS is no longer encapsulated by the PP (B) phases but is dispersed directly in the HDPE matrix. The PMMA (D) particles, on the other hand, are still encapsulated by the PS phases. It is probable that an even more striking change in the morphology from (PP/PS/PMMA) to (PP + PS/PMMA) would occur with additional amounts of added S–E.

CONCLUSIONS

The phase morphologies of quaternary blends of HDPE, PP, PS and PMMA can be correctly predicted by using our model based on the minimization of the total interfacial energy of the system. In every case examined, the predicted phase structure which is for an thermodynamically equilibrium state is in excellent agreement with the non-equilibrium, experimental morphology. This can be attributed to the fact that particle numbers which are determined by the interplay of shearing stresses, viscosities and interfacial tensions play only a minor role in influencing the energy level or the phase structure of the system. The phase structure is primarily determined by interfacial tensions. Our results further confirmed our previous conclusions[11] that the tendency for a polymer system to minimize its free energy is so strong that the phase structure having the lowest free energy level is formed even under the non-equilibrium mixing conditions.

The phase structure of a HDPE/PP/PS/PMMA blend

Figure 9 (a) TEM micrograph of an HDPE/PP/PS/PMMA 60/20/10/10 blend ($V_{PP}/V_{PS} = 2$); (b) TEM micrograph of an HDPE/PP/PS/PMMA 75/5/10/10 blend ($V_{PP}/V_{PS} = 0.5$) (A = HDPE, B = PP, C = PS, D = PMMA)

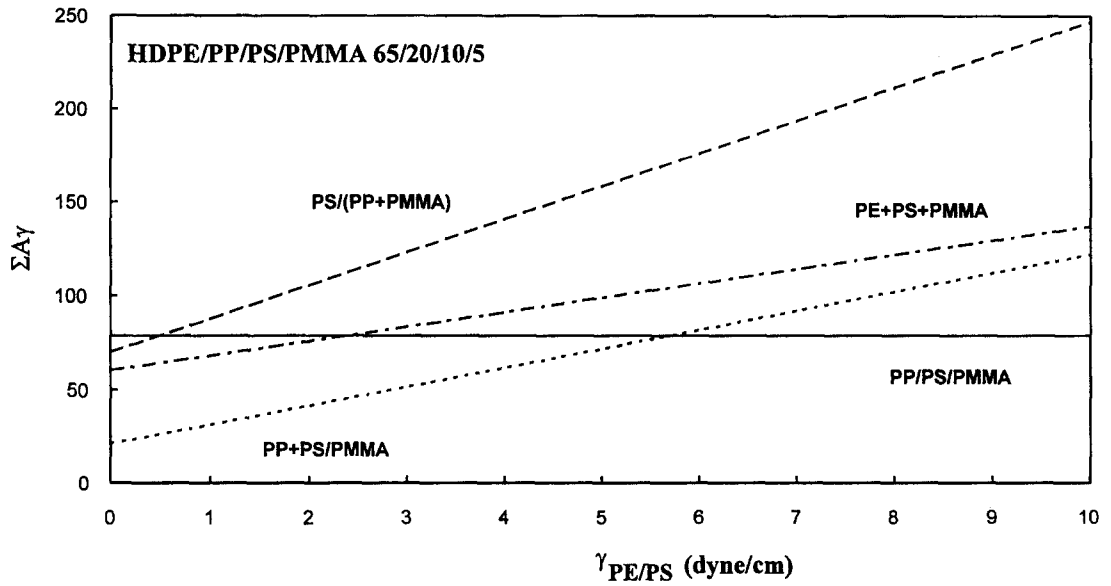

Figure 10 Interfacial energies ($\Sigma A_i \gamma_{ij}$) *versus* interfacial tension $\gamma_{HDPE/PS}$ for a quaternary blend of an HDPE/PP/PS/PMMA 65/20/10/5 blend

Figure 11 TEM micrograph of an HDPE/PP/PS/PMMA 65/20/10/5 blend (A = HDPE, B = PP, C = PS, D = PMMA)

Figure 12 TEM micrograph of an HDPE/PP/PS/PMMA 65/20/10/5 blend containing 0.5% w/w S–E block copolymer (A = HDPE, B = PP, C = PS, D = PMMA)

has been successfully changed from (PP/PS/PMMA) to (PP + PS/PMMA) by adding a small amount of an interfacially active S–E block copolymer to reduce the PE/PS interfacial tension. This result is also predicted by the model.

ACKNOWLEDGEMENTS

This work was supported by the National Institute of Standards and Technology under a Department of Commerce Advanced Technology Project grant. We thank Mr Kevin Battjes for his help with SEM and

TEM, and Ms Katherine Robertson for her help with photography. We are grateful to Dr S. Packirisamy for his synthesis of the S–E block copolymer.

REFERENCES

1. Hobbs, S. Y., Dekkers, M. E. J. and Watkins, V. H., *Polym. Bull.*, 1987, **17**, 341.
2. Hobbs, S. Y., Dekkers, M. E. J. and Watkins, V. H., *Polymer*, 1988, **29**, 1598.
3. Okamoto, M., Shinoda, Y., Kojima, T. and Inoue, T., *Polymer*, 1993, **34**, 4868.
4. Debier, D., Devaux, J. and Legras, R., *Polym. Eng. Sci.*, 1994, **34**, 613.
5. Cheng, T. W., Keskkula, H. and Paul, D. R., *Polymer*, 1992, **33**, 1606.
6. Cuerq, B. and Taha, M., *Polym. Networks Blends*, 1995, **5**, 95.
7. Guo, H. F., Gvozdic, N. J. and Meier, D. J., *PMSE Prepr.*, 1996, **74** (2).
8. Xanthos, M., Patel, A., Dey, S., Dagli, S. S., Jacob, C., Nosker, T. J. and Renfree, R. W., *Adv. Polym. Technol.*, 1994, **13**, 231.
9. Vivier, T. and Xanthos, M., *J. Appl. Polym. Sci.*, 1994, **54**, 569.
10. Vivier, T., Xanthos, M. and Breant, P., *ANTEC*, 93, 1227.
11. Guo, H. F., Packirisamy, S., Gvozdic, N. J. and Meier, D. J., *Polymer*, 1997, **38**, 785.
12. Wu, S., *Polymer Interface and Adhesion*, Marcel Dekker, New York, 1982.